Chinese Journal of Mechanical Engineering

ORIGINAL ARTICLE

Open Access

Effect of Initial Microstructure Prior to Extrusion on the Microstructure and Mechanical Properties of Extruded AZ80 Alloy with a Low Temperature and a Low Ratio

Hang Zhang[1], Haipeng Li[1], Rongguang Li[1], Boshu Liu[1*], Ruizhi Wu[2], Dongyue Zhao[2] and Shanshan Li[1*]

Abstract

Magnesium (Mg) alloys are the lightest metal structural material for engineering applications and therefore have a wide market of applications. However, compared to steel and aluminum alloys, Mg alloys have lower mechanical properties, which greatly limits their application. Extrusion is one of the most important processing methods for Mg and its alloys. However, the effect of such a heterogeneous microstructure achieved at low temperatures on the mechanical properties is lacking investigation. In this work, commercial AZ80 alloys with different initial microstructures (as-cast and as-homogenized) were selected and extruded at a low extrusion temperature of 220 °C and a low extrusion ratio of 4. The microstructure and mechanical properties of the two extruded AZ80 alloys were investigated. The results show that homogenized-extruded (HE) sample exhibits higher strength than the cast-extruded (CE) sample, which is mainly attributed to the high number density of fine dynamic precipitates and the high fraction of recrystallized ultrafine grains. Compared to the coarse compounds existing in CE sample, the fine dynamical precipitates of $Mg_{17}(Al, Zn)_{12}$ form in the HE sample can effectively promote the dynamical recrystallization during extrusion, while they exhibit a similar effect on the size and orientation of the recrystallized grains. These results can facilitate the designing of high-strength wrought magnesium alloys by rational microstructure construction.

Keywords Magnesium alloy, Low temperature and low ratio extrusion, Bimodal grain structure, Dynamic precipitate, Dynamic recrystallization

1 Introduction

In structural applications, wrought magnesium alloys are very attractive in terms of weight reduction, but their mechanical strength is relatively low at ambient temperatures [1–4]. In the recent works, researchers find that there is a synergistic effect between the coarse grains with a strong basal texture and submicron-sized grains with a weak texture, resulting in an increase in strength [5–7]. The idea of achieving the heterogeneous microstructures with high mechanical properties has received significant attention [8–11]. For example, a bimodal-grained AZ91 alloy prepared by hard-plate rolling exhibits a high ultimate tensile strength (UTS) of 370 MPa and a high elongation of 24% compared with the fine-grained AZ91 alloys [12]. A Mg-7Y-3Zn (wt.%) alloy with multimodal microstructure developed by extrusion shows a high UTS of 385 MPa and an elongation of 7% [13]. However, the strengthening mechanisms for the high strength of Mg alloys with heterogeneous microstructure still

*Correspondence:
Boshu Liu
liubs_syuct@126.com
Shanshan Li
shanshanli_work@126.com
[1] School of Mechanical and Power Engineering, Shenyang University of Chemical Technology, Shenyang 110142, China
[2] Key Laboratory of Superlight Materials & Surface Technology, Ministry of Education, Harbin Engineering University, Harbin 150001, China

lack systematic investigation. The strengthening effect from grain refinement is suggested to be enhanced with increasing volume fraction of recrystallized grains, but the decreasing volume fraction of deformed grains with strong texture will result in a loss of strength. Besides, the size and distribution of second-phase particles also play vital role on the strength of Mg alloys with heterogeneous microstructure. The precipitates not only directly influence the strengthening effect from second phase, but also affect the formation of heterogeneous microstructure [14–18]. Liao et al. reported that the precipitates with an average size of 1 μm in a Mg-1Gd-1Y-1Zn alloy affected the heterogeneous microstructure by particle stimulated nucleation (PSN) mechanism [15]. Zou et al. reported that the nano-sized precipitates (50 nm) in a Mg-5Zn-1Mn alloy suppressed dynamic recrystallization (DRX), resulting in a bimodal grain size distribution [16]. The influence of precipitates on DRX behavior depends on the deformation temperature because the interaction of dislocations and particles is temperature-dependent [17]. Thus, it is necessary to clarify the role of grain refinement, texture, and second phase on the strength of Mg alloys with different heterogeneous microstructure.

Extrusion is one of the most important processing methods for Mg and its alloys. Extrusion temperature and ratio play critical roles in the grain refinement of extruded Mg alloys. For example, the extrusion temperatures and ratio of AZ91 alloys are commonly controlled over 240 °C and 11, respectively, to achieve a homogeneous micron-scale microstructure [19–22]. The decreased extrusion temperature and extrusion ratio are suggested to reduce the recrystallization degree of extruded alloys and lead to a heterogeneous microstructure [23–26]. However, the effect of such a heterogeneous microstructure achieved at low temperatures on the mechanical properties is lacking investigation. Based on these works, we choose a commercial cast AZ80 alloy as initial material and design an extrusion process with low temperature (220 °C) and low ratio (4) to achieve heterogeneous microstructures. The extrusion ratio is chosen based on our previous works on extruded Mg alloys [19, 27], the selected ratio of 4 is suitable to achieve heterogeneous microstructure and ultrafine recrystallized grains. We compare the microstructure and mechanical properties of homogenized-extruded (HE) and cast-extruded (CE) AZ80 alloys. The role of grain refinement, texture, and second phase on the strength of AZ80 alloys are discussed in detail.

2 Experimental Procedures

In this work, a commercial AZ80 alloy with the actual composition of Mg-7.6Al-0.45Zn-0.27Mn (wt.%) was used. The composition was detected by inductively coupled plasma atomic emission spectrometry (ICP-AES). The cylindrical-shaped samples with a height of 100 mm and a diameter of 80 mm were cut from the billet. Some cylindrical samples were homogenized at 420 °C for 24 h and then quenched at room temperature. These as-cast and as-homogenized samples were heated to 220 °C and then extruded into the rods with a diameter of 40 mm, followed by a rapid quench into water at room temperature. The chamber temperature and mold temperature were both 240 °C. The extrusion ratio was set to 4. The ram velocity for extrusion was 0.2 mm/s. The details of extrusion processes are listed in Table 1. The cast-extruded and homogenized-extruded samples were marked as CE and HE samples, respectively.

Tensile bars with a gauge length of 25 mm and a diameter of 5 mm were tested at a strain rate of 10^{-3}/s at room temperature using a Shimadzu Autograph AG-I (100 kN). The tensile direction was parallel to the extrusion direction (ED), and three samples were tested under the same parameters. The microstructure was characterized with an OLS3000 optical microscope (OM), a FEI NOVA400 scanning electron microscope (SEM) and an Oxford HKL Channel 5 electron backscatter diffraction (EBSD) detector, as well as a JEOL JEM-2100F transmission electron microscope (TEM) with energy dispersive spectroscopy (EDS) detector. A mixed solution (2 g picric acid + 5 mL distilled water + 5 mL acetic acid + 4 mL nitric acid + 85 mL alcohol) was used for etching the specimens for OM and SEM observation. An accelerating voltage of 20 kV was used for the SEM and EBSD characterization. EBSD characterization was carried out using a step size of 0.6 μm. Kernel average misorientation map (KAM) is constructed based on the degree of misorientation between a measurement point (kernel) and all its surrounding neighbours [28]. EBSD samples were prepared by mechanical polishing followed by argon ion milling. The TEM characterization under high-angle annular dark field (HAADF) condition and EDS characterization were carried out at 200 kV. Thin-foil samples for TEM observation were prepared using low-energy ion beam thinning. The phase composition of the sample was examined by X-ray diffraction (XRD, Model D/Max 2500PC Rigaku) at 40 kV and a scanning speed of 4°/min. The sizes of grains and precipitates were obtained

Table 1 Processes of the extruded AZ80 alloys

Samples	Sample temperature (℃)	Chamber temperature (℃)	Mold temperature (℃)	Extrusion ratio (mm)	Extrusion speed (mm/s)
HE	220	240	240	4	0.2
CE	220	240	240	4	0.2

by Nano Measurer System 1.2 and derived from at least five images.

3 Results of Microstructure and Mechanical Properties

Figure 1 shows the microstructures of the HE and CE samples. As can be seen, bimodal-grained microstructure forms in the HE and CE samples. In the HE sample, the un-recrystallized elongated grains show an average length of 79 μm and an average width of 27 μm. The volume fraction of elongated grains in the HE sample is 68%. In comparison, elongated grains in the CE sample exhibit a smaller size (with an average length of 57 μm and an average width of 20 μm) but higher volume fraction (89%). Moreover, the elongated grains in the CE sample still have the dendritic morphology.

Figure 2 shows more details of the microstructures for the HE and CE samples. The images are obtained from the planes perpendicular to ED. Both in the HE and CE samples, the second-phase particles are mainly distributed between the coarse grains. In the HE sample, the average size of second-phase particles is 0.45 μm, and the second-phase particles homogenously distribute in the areas of DRXed grains (Figure 2c). These second-phase particles are the dynamic precipitates that form during the extrusion process because the alloying elements have been dissolved during homogenization treatment. Compared to the particles in the HE sample, the second-phase particles in the CE sample are coarse and concentrated (Figure 2f). It indicates that the second-phase particles in the CE sample form mainly during the solidification process of the as-cast alloy and are broken during the extrusion process. The XRD results are shown in Figure 3, which are used for investigating the phase composition of the extruded samples by varying the incident angle (θ). The results prove that the second phases in the HE and CE samples are mainly the $Mg_{17}(Al, Zn)_{12}$ phase, and the CE sample has a higher content of $Mg_{17}(Al, Zn)_{12}$ phase. Due to the $Mg_{17}(Al, Zn)_{12}$ phase in the HE sample is dynamically precipitated during extrusion, which means that the content of precipitates is restricted by the gap of solid solubility between the homogenizing temperature and extrusion temperature. In comparison, the $Mg_{17}(Al, Zn)_{12}$ phase in the CE sample forms during solidification

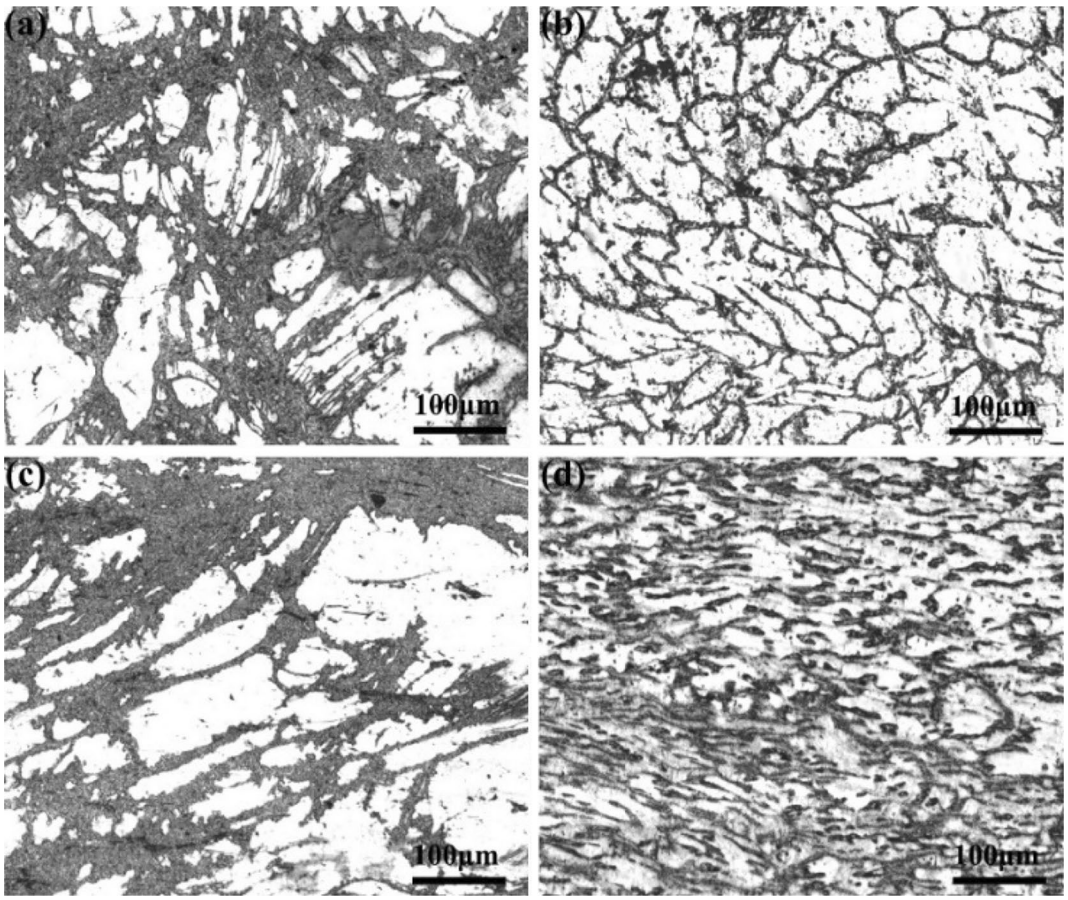

Figure 1 OM microstructure of the HE (**a** and **c**) and CE (**b** and **d**) samples: (**a** and **b**) Cross section, (**c** and **d**) Longitudinal section

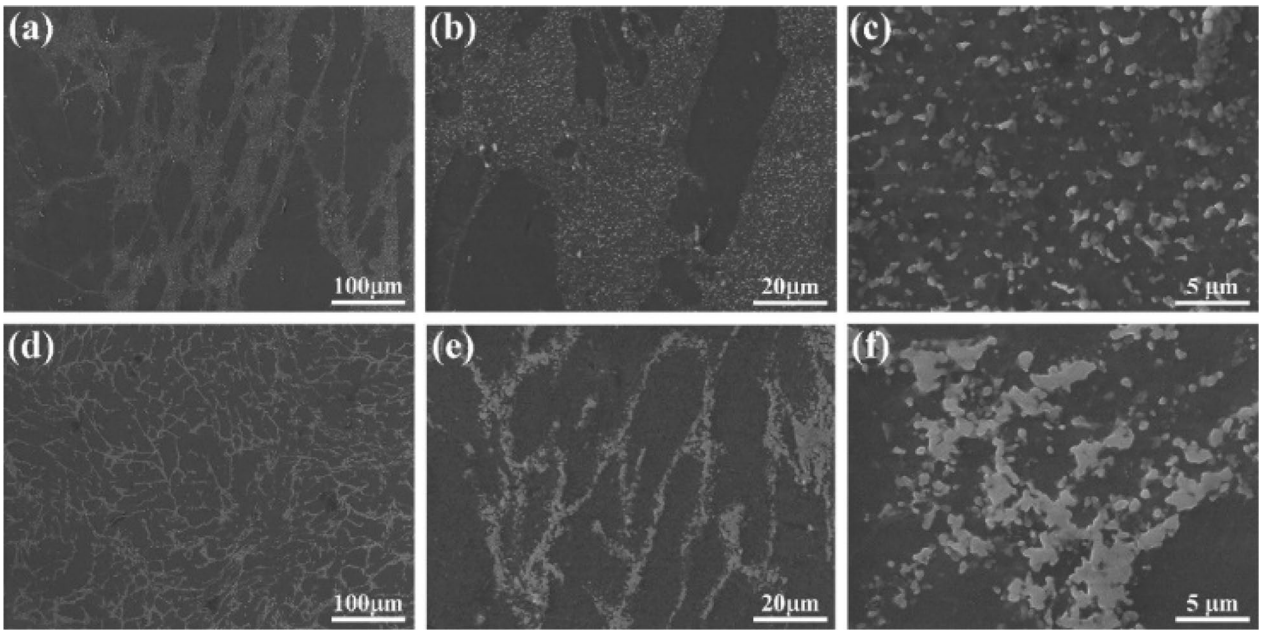

Figure 2 SEM images of the **a**-**c** HE and **d**-**f** CE samples

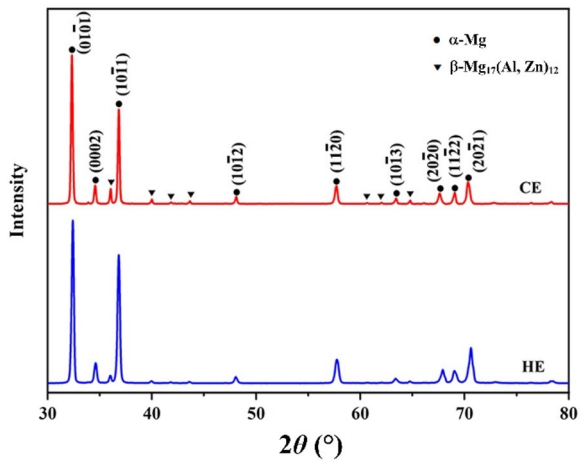

Figure 3 XRD pattern of the HE and CE samples

to room temperature, thus the concentration of solute atoms in the matrix is much higher and numerous second phases can be formed.

Figures 4 and 5 show the TEM images and EDS mapping results of the precipitates in the HE sample. The submicron-sized block-shaped and rod-shaped precipitates can be observed in the HE sample. The block-shaped phase is enriched with Al and Zn elements. The diffraction pattern in Figure 6 proves that the block-shaped phase is the $Mg_{17}(Al, Zn)_{12}$ phase, which is consistent with the XRD result. The TEM images in Figure 5 show the details of the diffusely distributed nano precipitates. The spherical precipitates have an average size of 18 nm. The rod-shaped precipitates exhibit an average width of 21 nm and an average length of 113 nm. These precipitates are enriched with Al and Mn elements. According to the works on Mg-Al-Zn system alloys [29], the precipitates should be the Al_8Mn_5 phase. As there are no diffraction peaks of Al_8Mn_5 phase can be detected in the XRD result (Figure 3), the volume fraction of Al_8Mn_5 phase should be quite low in the HE sample. In the CE sample, these second-phase particles are micron-sized, submicron-sized, and nano-sized particles, and almost no Al_8Mn_5 phase can be observed (Figure 7).

EBSD results (Figures 8 and 9) show the details of DRXed grains and texture of the HE and CE samples. The images are obtained from the planes perpendicular to ED. The sizes of the DRXed grains in the HE and CE samples are 0.8 μm and 0.7 μm, respectively. The microtextures of deformed and DRXed grains in the HE and CE samples are shown in Figures 2e and f. The deformed grains exhibit a strong basal texture in the HE and CE samples, and the recrystallized grains exhibit a weak texture. Such a heterogeneous texture is commonly observed in the Mg-Al-Zn alloys with heterogeneous recrystallized grain structures [5, 7–10, 30]. Due to the higher volume fraction of elongated grains, the texture of the CE sample is stronger than that of the HE sample. The KAM result (Figure 10) shows that the orientation gradient within the deformed region is larger than that in the DRXed grains. This is most likely caused by the high density of residual dislocations to

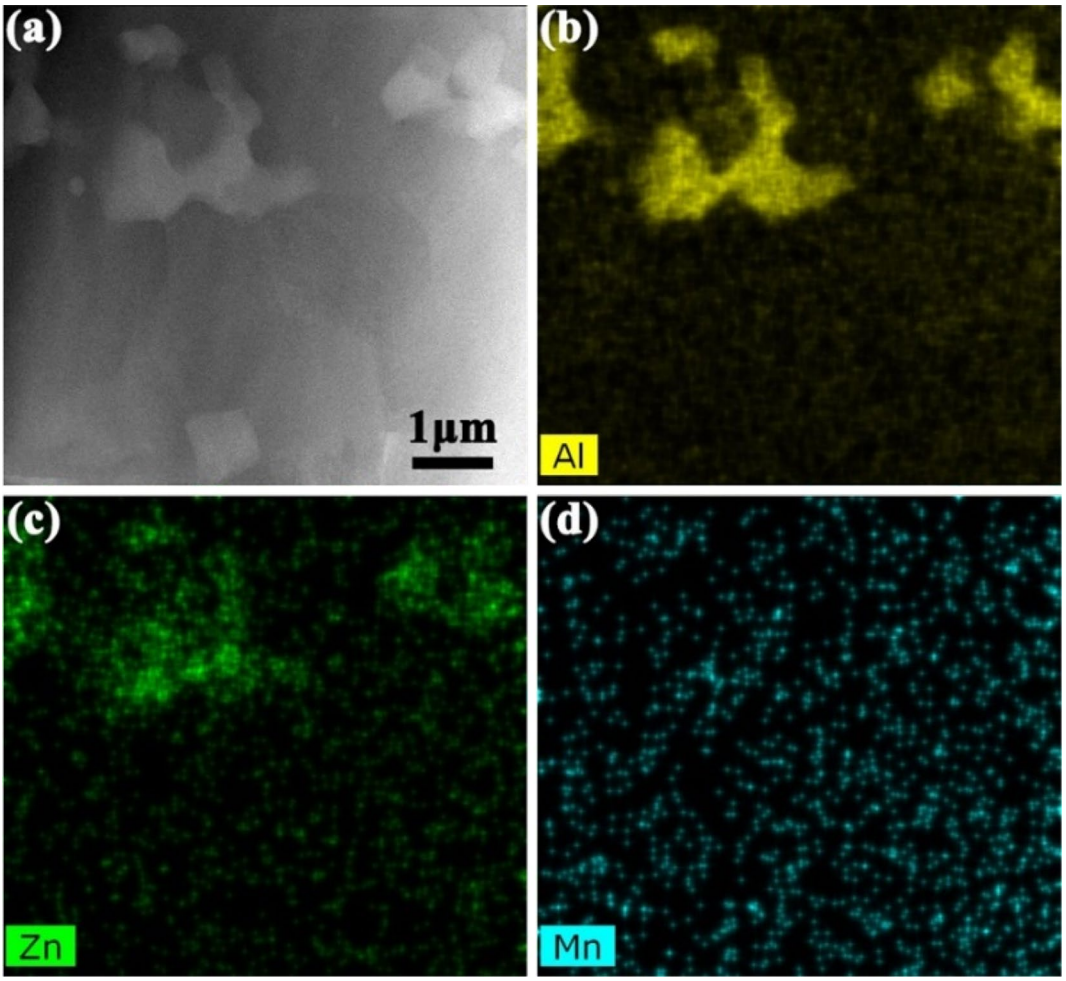

Figure 4 TEM images and EDS mapping results of the block-shaped precipitates in the HE sample: **a** HAADF image containing the dynamical precipitates, **b** Al element, **c** Zn element, **d** Mn element

accommodate the local lattice strain in the unDRXed grains. Accordingly, the average KAM value of deformed grains in the HE sample (0.64°) is lower than that in the CE sample (0.83°) because of the low volume fraction of unDRXed regions. The density of residual dislocations in the HE sample is thus identified to be lower than that in the CE sample.

The tensile properties of the HE and CE samples are shown in Figure 11. The corresponding yield strength (YS), ultimate tensile strength (UTS) and elongation are also listed. The YS, UTS, and elongation of the HE sample are 284 MPa, 331 MPa, and 4.8%, respectively. In contrast, the CE sample shows a lower YS (218 MPa) and UTS (315 MPa) but a comparable elongation (5.8%). The YS of the HE sample is significantly higher than that of the CE sample, but their ultimate tensile strength is quite close, which results from the stronger work-hardening ability of the CE sample than that of the HE sample.

4 Discussion on DRX Behavior and Strengthening Mechanism

As mentioned above, numerous tiny and dispersed precipitates exist in the HE sample, which are mainly formed during the extrusion process. It is suggested that strain-induced defects (such as dislocations and vacancies) can act as heterogeneous nucleation sites to promote dynamic precipitation [31]. A high density of dislocations and vacancies is induced during the extrusion process, which promotes the dynamic precipitation of second-phase particles with high number density. Meanwhile, the low extrusion temperature and the short time of the deformation process restricts the growth of these precipitates. According to the works on the effect of second-phase particles on the DRX behaviour of Mg-Al-Zn alloys [17, 32], the phase boundaries between

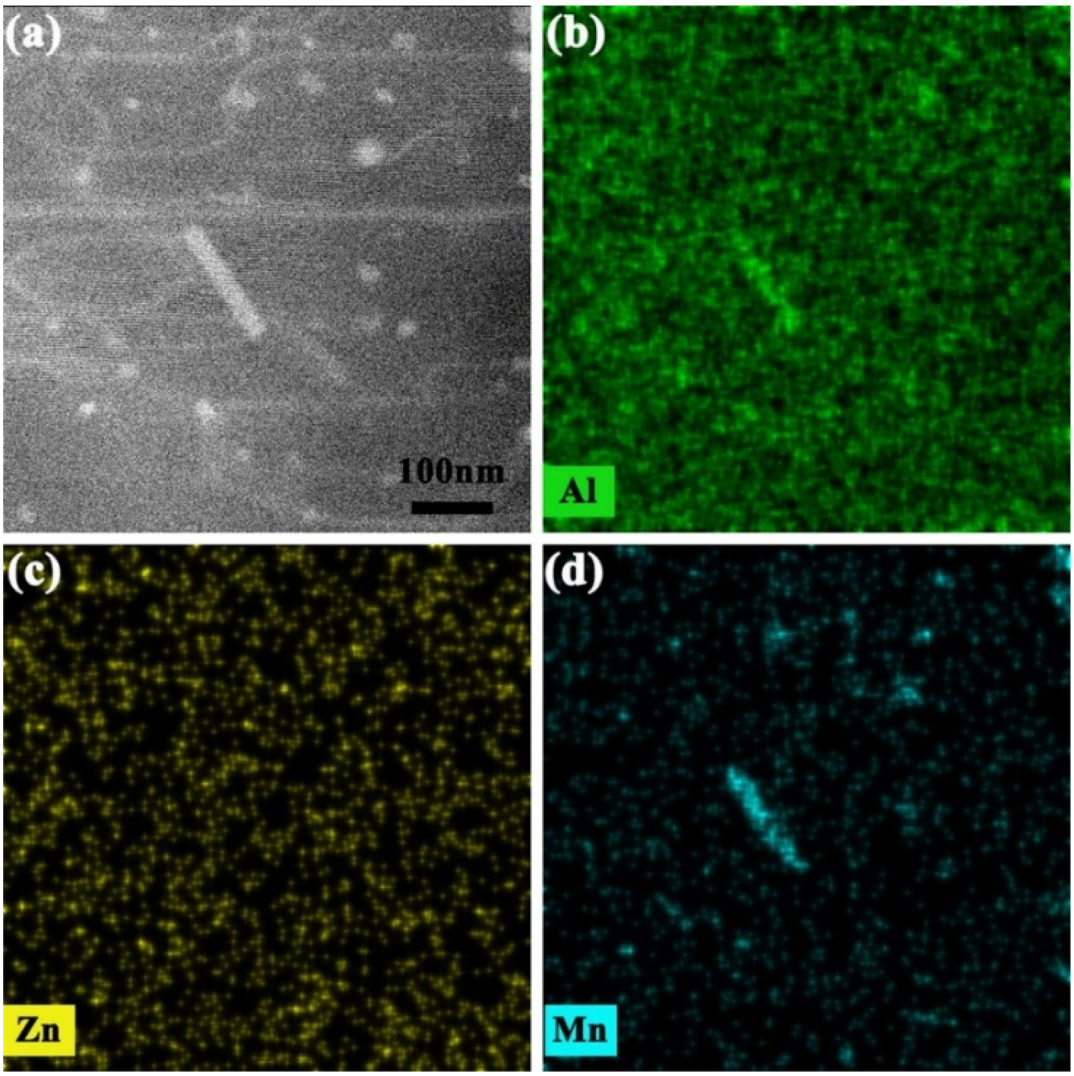

Figure 5 TEM images and EDS mapping results of the rod-shaped precipitates in the HE sample: **a** HAADF image containing the fine particles, **b** Al element, **c** Zn element, **d** Mn element

the second-phase particles and Mg matrix are the preferential sites for the nucleation of DRXed grains. In the present work, the number density of dynamically precipitated second-phase particles in the HE sample is significantly higher than that of the coarse compounds in the CE sample (Figure 2). It means that there are more phase boundaries exist in the HE sample than that in the CE sample, which facilitate the nucleation of DRXed grains. Thus, the HE sample achieves a higher volume fraction of DRX grains than the CE sample. Although the effects of the coarse compounds and the dynamically precipitated second-phase particle on the volume fraction of DRXed grains are quite different, the size and microtexture of the DRXed grains in the HE and CE samples are similar. It indicates that the coarse compounds and the dynamical precipitates have a similar influence on the size and orientation of DRXed grains in the present work. In this sense, the formation of ultrafine grains with weak texture in the HE and CE samples should be mainly attributed to the low extrusion temperature.

As shown in Figures 1 and 2, the HE sample has a higher volume fraction of DRXed grains, which will result in a stronger strengthening effect from grain refinement in the HE sample than that in the CE sample. Moreover, the high number density of the dynamic precipitates will also contribute to the strength of the HE sample. The formation of nano-size Al_8Mn_5 phase also improve the strength of the HE sample. Although the HE and CE samples have different grain size, texture, precipitates and DRX degree, the high density of dislocations that form during the low-temperature extrusion process result in the quite low

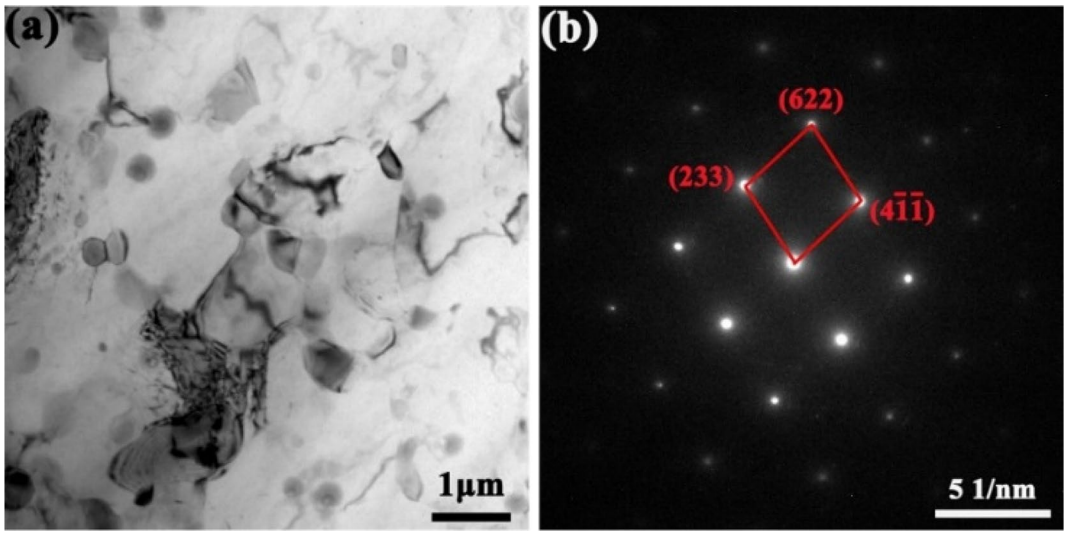

Figure 6 **a** TEM image of the dynamically precipitated particles in the HE sample and **b** the corresponding diffraction pattern

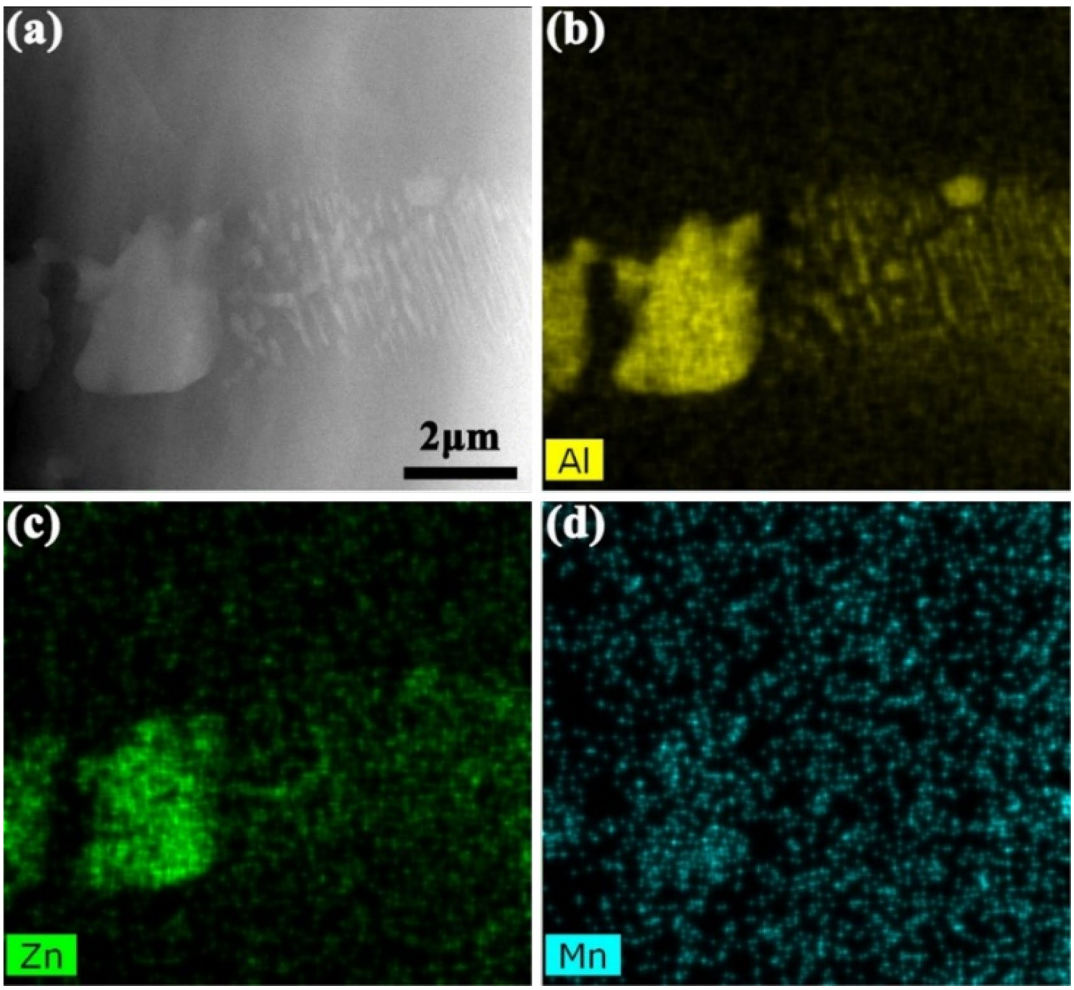

Figure 7 TEM images and EDS mapping results of precipitated in the CE sample: **a** HAADF image containing the fractured compounds formed during extrusion, **b** Al element, **c** Zn element, **d** Mn element

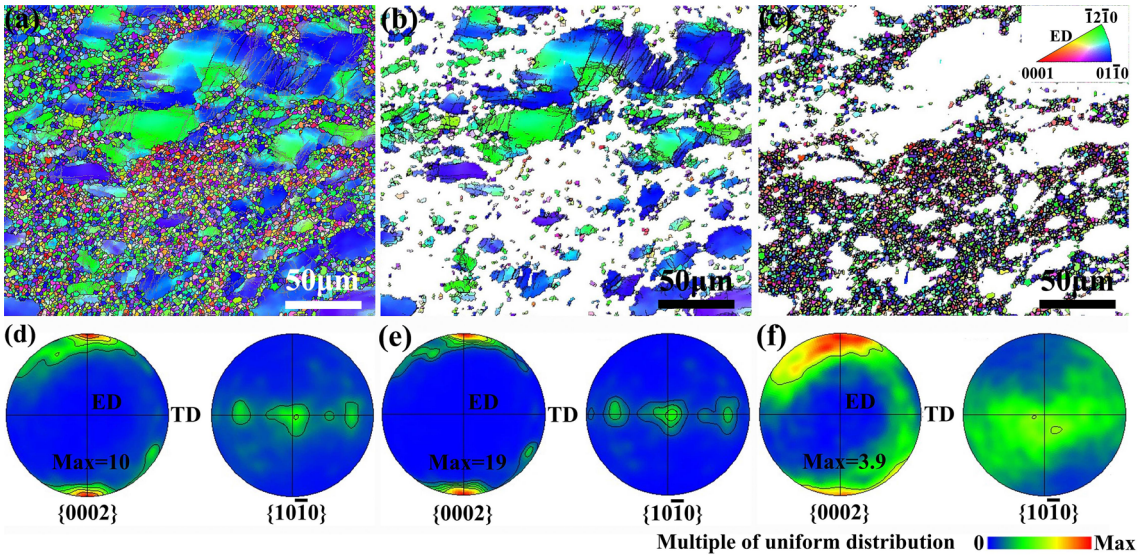

Figure 8 EBSD results of the HE sample: **a** IPF maps and **d** Microtextures of all grains, **b** IPF maps and **e** Microtextures of elongated grains, **c** IPF maps and **f** Microtextures of DRXed grains

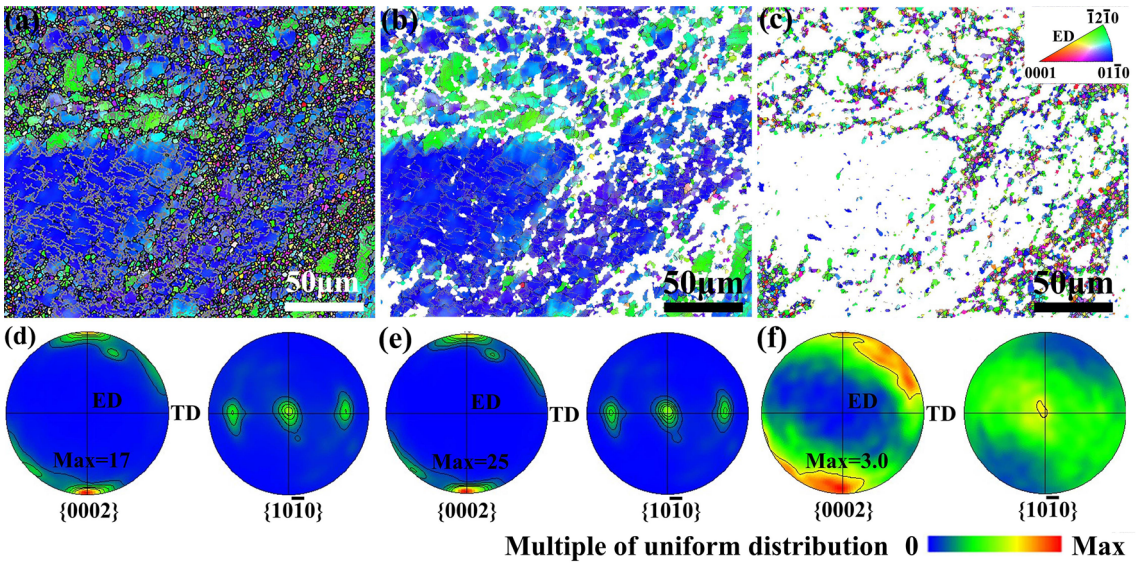

Figure 9 EBSD results of the CE sample: **a** IPF maps and **d** Microtexture of all grains, **b** IPF map and **e** Microtexture of elongated grains, **c** IPF map and **f** Microtexture of DRXed grains

elongation for both. It should be noted that the basal texture of the CE samples is stronger than that of the HE samples, and the residual dislocation density of the CE samples is higher than that of the HE samples, which will result in higher strengthening effect. However, the YS and UTS of the HE sample are still higher than those of the CE sample, indicating that the strengthening effects from grain refinement and dynamical precipitates are stronger than the strengthening effect from the texture in the extruded AZ80 alloys.

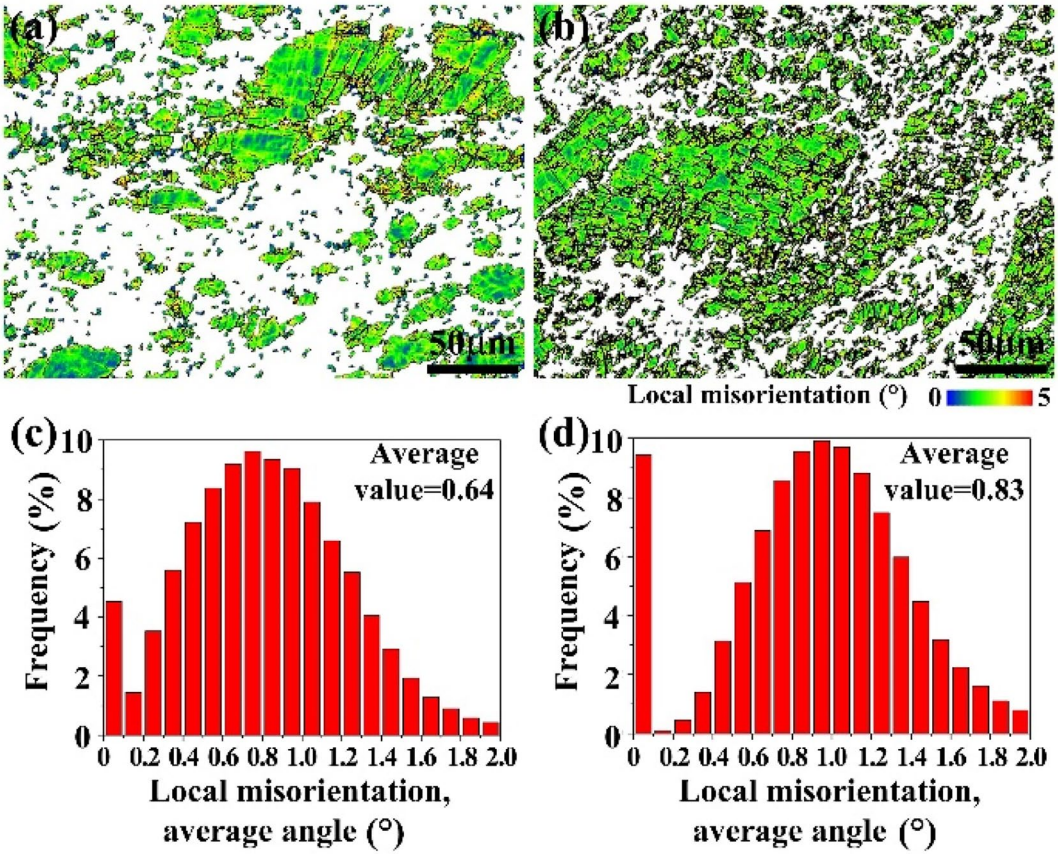

Figure 10 KAM maps and the distributions of average local misorientation angle of the deformed grains in the **a**, **c** HE and **b**, **d** CE samples

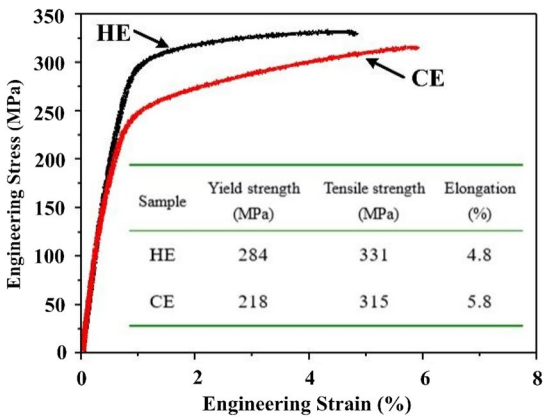

Figure 11 Engineering tensile stress-strain curves and tensile properties of the HE and CE samples

5 Conclusions

In the present work, the microstructure and mechanical properties of a commercial AZ80 alloy extruded at low temperature and low ratio are investigated. The main conclusions are:

(1) The HE sample shows a YS of 284 MPa, an UTS of 331 MPa, and an elongation of 5.8%. In contrast, the CE sample exhibits lower YS (218 MPa), UTS (315 MPa), and elongation of 4.8%.
(2) The higher YS and UTS of the HE sample are mainly attributed to the ultrafine DRXed grains with a high volume fraction and the dynamical precipitates of $Mg_{17}(Al, Zn)_{12}$ with a high number density.
(3) Compared to the coarse compounds existing in CE sample, the fine dynamical precipitates of $Mg_{17}(Al, Zn)_{12}$ are formed in the HE sample, which promotes effectively the dynamical recrystallization during extrusion, while they exhibit a similar effect on the size and orientation of the recrystallized grains.

Acknowledgements
Not applicable.

Author Contributions
RL was in charge of the whole trial; HZ, BL, and SL wrote the manuscript; HL, RW, and DZ assisted with sampling and laboratory analyses. All authors read and approved the final manuscript.

Authors' Information
Hang Zhang, born in 1991, is currently an associate professor at *School of Mechanical and Power Engineering, Shenyang University of Chemical Technology, Shenyang, China.* His main research interests include high-strength magnesium alloy and strengthening mechanisms of magnesium alloy.
Haipeng Li, born in 1997, is currently a master candidate at *School of Mechanical and Power Engineering, Shenyang University of Chemical Technology, Shenyang, China.*
Rongguang Li, born in1980, is currently a professor at *School of Mechanical and Power Engineering, Shenyang University of Chemical Technology, Shenyang, China.* His main research interests include high-strength magnesium alloy and strengthening mechanisms of magnesium alloy.
Boshu Liu, born in 1992, is currently an associate professor at *School of Mechanical and Power Engineering, Shenyang University of Chemical Technology, Shenyang, China.* Her main research interests include high-strength magnesium alloy and strengthening mechanisms of magnesium alloy.
Ruizhi Wu, born in 1977, is currently a professor at *Key Laboratory of Superlight Materials & Surface Technology, Ministry of Education, Harbin Engineering University, Harbin, China.* His main research interests include the microstructure control and strengthening mechanisms of Mg alloy and Al alloy.
Dongyue Zhao, born in 1996, is currently a PhD candidate at *Key Laboratory of Superlight Materials & Surface Technology, Ministry of Education, Harbin Engineering University, Harbin, China.*
Shanshan Li, born in 1993, is currently an associate professor at *School of Mechanical and Power Engineering, Shenyang University of Chemical Technology, Shenyang, China.* Her main research interests include high-strength magnesium alloy and strengthening mechanisms of magnesium alloy.

Funding
Supported by National Natural Science Foundation of China (Grant Nos. 52171121, 51971151, 52201131 and 52201132), Liaoning Provincial Xingliao Program of China (Grant No. XLYC1907083), Liaoning Provincial Natural Science Foundation of China (Grant No. 2022-NLTS-18-01), Open Foundation of Key Laboratory of Superlight Materials and Surface Technology of Ministry of Education of China (Grant No. HEU10202205).

Data Availability Statement
The datasets used and/or analyzed during the current study are available from the corresponding author on reasonable request.

Declarations

Competing Interests
The authors declare no competing financial interests.

Received: 4 December 2022 Revised: 11 May 2023 Accepted: 16 May 2023
Published online: 21 June 2023

References

[1] Y Yang, X M Xiong, J Chen, et al. Research advances in magnesium and magnesium alloys worldwide in 2020. *Journal of Magnesium and Alloys*, 2021, 9(3): 705-747.
[2] J H Zhang, S J Liu, R Z Wu, et al. Recent developments in high-strength Mg-RE-based alloys: Focusing on Mg-Gd and Mg-Y systems. *Journal of Magnesium and Alloys*, 2018, 6(3): 277-291.
[3] H Zhang, H L Hao, G Y Fu, et al. Microstructure and mechanical property of hot-rolled Mg-2Ag alloy prepared with multi-pass rolling. *Acta Metallurgica Sinica (English Letters)*, 2023, 36: 335-342.
[4] B N Wang, F Wang, Z Wang, et al. Compressive deformation behavior of ultrafine-grained Mg-3Zn-1.2Ca-0.6Zr alloy at room temperature. *Journal of Alloys and Compounds*, 2021, 871: 159581.
[5] J W Kang, X F Sun, K K Deng, et al. High strength Mg-9Al serial alloy processed by slow extrusion. *Materials Science and Engineering: A*, 2017, 697: 211-216.
[6] Z J Zhang, L Yuan, D B Shan, et al. The quantitative effects of temperature and cumulative strain on the mechanical properties of hot-extruded AZ80 Mg alloy during multi-directional forging. *Materials Science and Engineering: A*, 2021, 827: 142036.
[7] Z F Li, J Dong, X Q Zeng, et al. Influence of Mg17Al12 intermetallic compounds on the hot extruded microstructures and mechanical properties of Mg-9Al-1Zn alloy. *Materials Science and Engineering: A*, 2007, 466(1-2): 134-139.
[8] Z D Zhao, Q Chen, Y B Wang, et al. Microstructures and mechanical properties of AZ91D alloys with Y addition. *Materials Science and Engineering: A*, 2009, 515(1-2): 152-161.
[9] Z Z Jin, M Zha, Z Y Yu, et al. Exploring the Hall-Petch relation and strengthening mechanism of bimodal-grained Mg-Al-Zn alloys. *Journal of Alloys and Compounds*, 2020, 833: 155004.
[10] H Zhang, H Y Wang, J G Wang, et al. The synergy effect of fine and coarse grains on enhanced ductility of bimodal-structured Mg alloys. *Journal of Alloys and Compounds*, 2019, 780: 312-317.
[11] Z J Li, J G Wang, R F Yan, et al. Effect of Ce addition on hot deformation behavior and microstructure evolution of AZ80 magnesium alloy. *Journal of Materials Research and Technology*, 2022, 16: 1339-1352.
[12] H Y Wang, Z P Yu, L Zhang, et al. Achieving high strength and high ductility in magnesium alloy using hard-plate rolling (HPR) process. *Scientific Reports*, 2015, 5: 17100.
[13] M Yamasaki, K Hashimoto, K Hagihara, et al. Effect of multimodal microstructure evolution on mechanical properties of Mg-Zn-Y extruded alloy. *Acta Materialia*, 2011, 59(9): 3646-3658.
[14] P Prakash, M A Wells, B W Williams. Hot deformation of cast AZ31 and AZ80 magnesium alloys-Influence of Al content on microstructure and texture development. *Journal of Alloys and Compounds*, 2022, 897: 162876.
[15] H X Liao, J H Kim, J B Lv, et al. Microstructure and mechanical properties with various pre-treatment and Zn content in Mg-Gd-Y-Zn alloys. *Journal of Alloys and Compounds*, 2020, 831: 154873.
[16] J K Zou, J H Chen, H G Yan, et al. Effects of Sn addition on dynamic recrystallization of Mg-5Zn-1Mn alloy during high strain rate deformation. *Materials Science and Engineering: A*, 2018, 735: 49-60.
[17] F J Humphreys. *Recrystallization and related annealing phenomena*. Oxford: Elsevier, 2002.
[18] J S Xie, Z Zhang, S J Liu, et al. Designing new low alloyed Mg-RE alloys with high strength and ductility via high-speed extrusion. *International Journal of Minerals, Metallurgy and Materials*, 2023, 30(1): 82-91.
[19] R G Li, H R Li, D Zhao, et al. High strength commercial AZ91D alloy with a uniformly fine-grained structure processed by conventional extrusion. *Materials Science and Engineering: A*, 2020, 780: 139193.
[20] X Che, Q Wang, B B Dong, et al. The evolution of microstructure and texture of AZ80 Mg alloy cup-shaped pieces processed by rotating backward extrusion. *Journal of Magnesium and Alloys*, 2021, 9(5): 1677-1691.
[21] G L Shi, K Zhang, X G Li, et al. Dislocation configuration evolution during extension twinning and its influence on precipitation behavior in AZ80 wrought magnesium alloy. *Journal of Magnesium and Alloys*, 2021. https://doi.org/10.1016/j.jma.2021.08.032.
[22] X Zhao, P C Gao, G Chen, et al. Effects of aging treatments on low-cycle fatigue behavior of extruded AZ80 for automobile wheel disks. *Materials Science and Engineering: A*, 2021, 799: 140366.
[23] B N Wang, F Wang, Z Wang, et al. Microstructure and mechanical properties of Mg-Zn-Ca-Zr alloy fabricated by hot extrusion-shearing process. *Materials Science and Engineering: A*, 2020, 795: 139937.
[24] K B Nie, Z H Zhu, K K Deng, et al. Effect of extrusion temperature on microstructure and mechanical properties of a low-alloying and ultra-high strength Mg-Zn-Ca-Mn matrix composite containing trace TiC nanoparticles. *Journal of Magnesium and Alloys*, 2020, 8(3): 676-691.
[25] Y X Niu, Z T Song, Q C Le, et al. Excellent mechanical properties obtained by low temperature extrusion based on Mg-2Zn-1Al alloy. *Journal of Alloys and Compounds*, 2019, 801: 415-427.
[26] Z Zhang, J H Zhang, J Wang, et al. Toward the development of Mg alloys with simultaneously improved strength and ductility by refining grain size via the deformation process. *International Journal of Minerals, Metallurgy and Materials*, 2021, 28: 30-45.
[27] R G Li, H R Li, H C Pan, et al. Achieving exceptionally high strength in binary Mg-13Gd alloy by strong texture and substantial precipitates. *Scripta Materialia*, 2021, 193: 142-146.

[28] A Clair, M Foucault, O Calonne, et al. Strain mapping near a triple junction in strained Ni-based alloy using EBSD and biaxial nanogauges. *Acta Materialia*, 2011, 59(8): 3116-3123.
[29] Y Tamura, Y Kida, H Tamehiro, et al. The effect of manganese on the precipitation of Mg17Al12 phase in magnesium alloy AZ91. *Journal of Materials Science*, 2008, 43(4): 1249-1258.
[30] M Zha, H Zhang, C Wang, et al. Prominent role of a high volume fraction of Mg17Al12 particles on tensile behaviors of rolled Mg-Al-Zn alloys. *Journal of Alloys and Compounds*, 2017, 728: 682-693.
[31] X Ma, S E Prameela, P Yi, et al. Dynamic precipitation and recrystallization in Mg-9wt.% Al during equal-channel angular extrusion: A comparative study to conventional aging. *Acta Materialia*, 2019, 172: 185-199.
[32] T Al-Samman. Modification of texture and microstructure of magnesium alloy extrusions by particle-stimulated recrystallization. *Materials Science and Engineering: A*, 2013, 560: 561-566.